Remote Sensing of Environment 171 (2015) 33–44

Contents lists available at ScienceDirect

Remote Sensing of Environment

journal homepage: www.elsevier.com/locate/rse

Optimum spectral and geometric parameters for early detection of laurel wilt disease in avocado

A.I. De Castro [a], R. Ehsani [a,*], R. Ploetz [b], J.H. Crane [b], J. Abdulridha [a]

[a] Citrus Research and Education Center, University of Florida, IFAS, 700 Experiment Station Road, Lake Alfred, FL 33850, USA
[b] Tropical Research and Education Center, University of Florida, 18905 SW 280th St., Homestead, 33031 FL, USA

ARTICLE INFO

Article history:
Received 6 March 2015
Received in revised form 31 August 2015
Accepted 22 September 2015
Available online 24 October 2015

Keywords:
Laurel wilt
Avocado
Spectral analysis
Aerial image
Vegetation indices
Early disease detection
Precision agriculture

ABSTRACT

Avocado (*Persea americana*) is a crop that is second in importance in Florida behind citrus with a wholesale value of $35 million and represents approximately 60% of the tropical fruit crop acreage. Laurel wilt (LW) is a lethal disease that has spread rapidly along the southeastern seaboard of the United States affecting commercial avocado production. This article evaluates the spatial and spectral requirements for quick and accurate detection of LW. Spectral data from healthy (H), Phytophthora root rot (PPR) and LW leaves were analyzed using ANOVA and two neural networks, multilayer perceptron (MLP) and radial basis function (RBF). The most effective wavelengths were identified and the filters were updated to a MCA-6 Tetracam camera (580–10 nm, 650–10 nm, 740–10 nm, 750–10 nm, 760–10 nm and 850–40 nm). Then, the MCA camera was used to take multispectral aerial images from a helicopter at three altitudes (180, 250 and 300 m) in an avocado field with trees at different stages of LW development, early, intermediate and late. The analyses were conducted based upon 2-class and 4-class systems. The 2-class system was designed to differentiate H and LW trees sufficient to identify trees for removal and the 4-class system was used to differentiate H plants and the three stages of LW development. Aerial image analysis proved the utility of the selected filters for successful identification of LW, even for trees in early stage of disease development with minimal symptoms. The ideal flight altitude of 250 m (15.3 cm pixel size) was selected according to the M-values and biological parameters such as canopy size and orchard size. The optimum VIs determined by higher M-values were $TCARI_{760-650}$ as well as GNDVI, NIR/G, Redge/G and VIGreen using any of the bands related to Redge (740 and 750 nm) or NIR regions (760 and 850 nm). Results reported on the utility of the 2-class and 4-class systems using the above VIs to discriminate LW; however it would be more convenient to develop the algorithm based on the 4-class system (H, early, intermediate and late). The early detection of LW through the methodology proposed in this research could allow farmers to control the movement of this disease through proper management strategies.

1. Introduction

Avocado (*Persea americana*) is an important fruit crop in Florida. It is second in importance in Florida behind citrus, with 30,700 t of fruit harvested in 2013 for a wholesale value of $35 million (Evans & Bernal Lozano, 2015). Fruit worth $24.4 million a year at the farm gate (USDA, 2013) are produced by 500 growers and handled by 30 registered avocado shippers (Flinn, 2014). This industry represents approximately 60% of the tropical fruit crop acreage in Florida (2800 ha), of which over 98% occurs in southeastern Miami-Dade County (Ploetz et al., 2012; USDA, 2014). Avocado production brings in substantial "new dollars" to Florida ($100 million per annum) (Evans & Bernal Lozano, 2015). Avocado trees form an important part of the urban canopy; backyard trees contribute economic, esthetic, and environmental benefits, adding as much as 10% to residential property values in South Florida (Evans & Crane, 2012). There are more than 250,000 urban avocado trees in the state of Florida (Pybas, 2009).

Avocado is the most important agricultural suscept of laurel wilt (Ploetz et al., 2011a). Laurel wilt (LW) is a lethal and complex disease that has spread rapidly along the southeastern seaboard of the United States since it was first reported in the Western Hemisphere in 2002 in Port Wentworth, Georgia (Ploetz, Hulcr, Wingfield, & de Beer, 2013; Rabaglia, Dole, & Cognato, 2006). In February 2011, LW was confirmed for the first time in Miami-Dade County, 10 miles north of Florida's main avocado production area in Homestead (Ploetz et al., 2011b). In 2012, it was first detected in the commercial avocado production area (CAPA) (Ploetz et al., 2013). By the end of 2014, the disease had been confirmed as far west as Claiborne County, LA, as far north as Sampson County, NC, and as far south as Miami-Dade County, FL (USDA, 2014). The rapid movement of LW has been due to the pathogen's mobile ambrosia beetle vectors, human transport of infested wood (e.g., firewood), and the presence of native and non-native plants susceptible to ambrosia beetle attack and laurel wilt throughout the

* Corresponding author.
E-mail address: ehsani@ufl.edu (R. Ehsani).

http://dx.doi.org/10.1016/j.rse.2015.09.011

southeastern United States (Chemically Speaking Newsletter, 2009; Ploetz et al., 2011a).

LW is a recently introduced vascular disease caused by the Asian fungus *Raffaelea lauricola*, which has ambrosia beetle vectors, including *Xyleborus glabratus* (Fraedrich et al., 2008; Ploetz et al., 2012; Harrington, Fraedrich, & Aghayeva, 2008). The presence of the LW pathogen results in vascular plugging of the xylem, beginning as soon as three days after infection, thereby impeding the flow of water and nutrients (Ploetz et al., 2013). Wilting occurs soon after, with leaves rapidly changing from an oily green color to brown, and defoliation occurs within 2–3 months of the onset of symptoms (Ploetz et al., 2012). Many symptoms of LW are similar to those caused by other diseases or factors, such as freeze damage, Phytophthora root rot, Verticillium wilt, lightening and fruit stress (overbearing), which makes visual diagnosis of the disease difficult (Sankaran, Ehsani, Inch, & Ploetz, 2012). In addition, it is difficult to manage the disease once plants display external symptoms, since they develop only after significant colonization of the host by the pathogen occurs and fungicide movement and efficacy is dramatically reduced in such trees (Inch & Ploetz, 2012; Ploetz et al., 2011b). Thereby, the early detection of LW (trees with minimum symptoms) could be a valuable source of information for executing proper disease control measures to prevent the development and the spread of the disease (Sankaran, Mishra, Ehsani, & Davis, 2010).

While other diseases can kill avocado trees, none of them develop as quickly as LW (Ploetz et al., 2012). In Florida, it is estimated that losses of $27 to 54 million could occur if reliable control strategies are not developed (Evans, Crane, Hodges, & Osborne, 2010; Ploetz et al., 2012), while the cost to replace trees destroyed by the disease would be around $423 million (Evans & Crane, 2012). Moreover, there is a major concern that LW will spread to California, the leading producer in the United States, and Mexico, the world's top producer (Evans et al., 2010; FAO, 2010; Ploetz et al., 2012).

Sanitation is an important step in managing LW (Ploetz & Carrillo, in press), but accurate and rapid measures are lacking (Sankaran et al., 2012). Currently, symptomatic trees are detected, infection by *R. lauricola* is confirmed via laboratory analyses, and positive trees are removed and destroyed as quickly as possible. An early detection technique to replace this time-consuming and expensive method could be quite useful in mitigating the development and spread of this disease (De Castro, Ehsani, Ploetz, Crane, & Buchanon, 2015). Sankaran et al. (2012) proved that LW could be detected with visible-near infrared spectral reflectance data from leaves of *R. lauricola*-infected plants, even asymptomatic or trees with minimum symptoms.

By applying multivariate analysis tools, such as neural networks, it is possible to detect significant spectral difference and classify spectral data into agronomical classes (De Castro, Jurado-Expósito, Peña-Barragán, & López-Granados, 2012; Han, Kamner, & Pei, 2012). Neural networks, together with naïve Bayesian classifier, support vector machines, and decision trees, are considered the more advanced techniques for data classification (Han et al., 2012). Neural networks allow the exploration of relationships or models that could not be detected using traditional statistical procedures (Rzempoluck, 1997). Furthermore, neural networks offer some advantages over those advanced techniques, such as high flexibility and adaptability to the results, high tolerance of noisy data and errors, ability to classify non-trained patterns, capacity to work when low knowledge of relationships between attributes and classes conditions exist, and high computation process speed (Han et al., 2012). Those advantages contribute to make neural networks one of the most useful classification predictors in data mining (Rogan et al., 2008). Neural networks and spectral data have been previously used in a wide array of real-world data, such as estimating crop areas (Heremans, Bossyns, Eerens, & Van Orshoven, 2011), mapping land-cover modifications (Rogan et al., 2008), and selecting a subset of several wavelengths or vegetation indices for detection of biotic and abiotic stresses in plants (De Castro et al., 2012; Estep, Terrie, & Davis, 2004; Wu, Liu, Zhou, Yan, & Zhang, 2012).

Usha and Singh (2013) and Sankaran et al. (2010) reviewed the potential for image-based remote sensing to detect diseases of crops. Multispectral aerial imaging has been used to detect, monitor and quantify diseases of tomatoes (Zhang, Qin, & Liu, 2005), winter wheat (Dammer, Möller, Rodemann, & Heppner, 2011), creeping bentgrass (Raikes & Burpee, 1998), cranberries (Pozdnyakova, Oudemans, Hughes, & Giménez, 2012), olives (Calderón, Navas-Cortés, Lucena, & Zarco-Tejada, 2013) and citrus (Du, Chang, Yang, & Srilakshmid, 2008; García-Ruiz et al., 2013). Remote sensing tools can significantly improve disease detection if the spectral and spatial properties of remote sensing equipment are sufficient to detect differences in spectral reflectance (López-Granados, 2011). Some authors have evaluated image spatial and/or spectral properties required for agriculture applications. For example, García-Ruiz et al. (2013) studied the effect of image resolution on classification performance by comparing a multi-band imaging sensor with a hyperspectral imaging system to detect Huanglongbing in citrus; better accuracies in classification were obtained when high-resolution multi-band images where used. Sankaran, Khot, Maja, and Ehsani (2013) and Torres-Sánchez, López-Granados, De Castro, and Peña-Barragán (2013) tested spectral and spatial properties of imagery sets taken at different altitudes to detect stress in citrus orchards and discriminate weed seedlings. Gray, Shaw, Gerard, and Bruce (2008) concluded that high spatial and spectral resolutions were needed to detect early season weeds in multispectral images of soybean fields. Successful image analyses clearly rely on defining the correct spatial and spectral resolution.

De Castro et al. (2015) reported on the utility of red-edge, green and blue aerial images to detect LW on avocado. They confirmed that the contrast between visible bands was enough for the accurate discrimination of a tree affected by LW once external symptoms had fully developed. However, they suggested that a higher spectral resolution camera with a greater band number and narrower wavelengths would be needed to detect infection by *R. lauricola* before symptoms developed.

The objective of the present study was to evaluate the spatial and spectral requirements for quick and accurate detection of LW for the future purpose of developing a LW classification algorithm. The research was divided in two parts; in the first part of this study, spectral analysis was carried out under controlled conditions, and in the second part, image analysis was performed at canopy level in a commercial avocado field. The specific goals were to: i) select the best multispectral wavebands to efficiently discriminate affected trees and select those filters to attach to a multiband camera; ii) quantify the influence of image spatial resolution (i.e. flight altitude) in the detection of affected trees; and iii) establish the best vegetation indices and number of classes in order to develop the classification algorithm.

2. Material and methods

2.1. Part 1: laboratory data—spectral analysis

2.1.1. Host inoculation

Leaves were obtained from potted 'Simmonds' avocado trees grown in a temperature-controlled greenhouse at the University of Florida's Tropical Research and Education Center (TREC) in Homestead. To induce LW, 10 plants were inoculated approximately 5 cm above the soil level by drilling four small holes around the circumference of the trunk, each of which received 750 conidia of *R. lauricola*, for a total of 3000 plant^{-1}. By 14 days after inoculation (DAI), slightly early symptoms of LW had begun to develop in some of the leaves. To induce Phytophthora root rot (PRR), 10 plants were inoculated by infesting each of 10 pots with 6 g of wheat seed colonized with *Phytophthora cinnamomi*. After 14 days, early symptoms of PRR appeared in the form of yellowing of some leaves. For comparison, healthy (H) leaves were obtained from potted plants grown in full sun.

Samples were kept in sealed Ziploc® bags in a cooler and brought to the lab for spectral measurements and virus testing (Naidu, Perry, Pierce, & Mekuria, 2009).

2.1.2. Spectral reading

Four leaves per plant were sampled from each of 10 H and the inoculated plants, 14 DAI. Asymptomatic and slightly affected leaves, just beginning to lose turgidity, were selected from LW plants. Spectral reflectance data were collected under controlled laboratory conditions in the TREC with a handheld spectroradiometer (SVC HR-1024 spectroradiometer, Spectra Vista Corporation) at 50 cm height above each leaf with a 4° field-of-view optical lens in the spectral range of 350 to 2500 nm (Fig. 1). The measurements were made within 3 h after the leaves were collected (Naidu et al., 2009). Five reflectance spectra were collected for each leaf. A spectral range of 400 to 950 nm with 10 nm spectral resolution was used based on published recommendations (Ray et al., 2010) and the availability of commercial waveband filters that would enable the development of a cost-effective sensor. For each sample, 45 spectral reflectance features were analyzed. Fig. 2 shows the spectral variability in the visible range for 10 nm averaged H, LW and PPR leaf reflectance 14 days after inoculation (DAI). The spectral signature for those classes showed overlap areas in much of the visible spectrum from 400 to 700 nm (Fig. 1). Two portable halogen work lamps (500 W) were used as the light source, and the reference reflectance spectra were acquired using a white panel (Spectralon Reflectance Target, CSTM-STR-99–100; Spectra Vista Corporation) in the presence of the light source (Fig. 3).

2.1.3. Data analysis and band selection

Spectral data for LW, PRR and H plants were analyzed with Tukey's studentized range test ($\alpha = 0.01$) (JMP 10, SAS Institute Inc., Campus Drive, Cary, NC, USA 27513), and results were used to select filters for future image analyses.

2.1.3.1. Neural networks. Two neural networks, multilayer perceptron (MLP) and radial basis function (RBF), were applied to identify the best 10 nm bandwidth for discrimination of H and LW trees. A neural network is a function of predictors, also called inputs or independent variables, that minimize the prediction error of target variables, also called outputs (SPSS Manual). These models are able to learn by example. Thus, when using a neural network there is no need to program how the output is obtained given certain input; rather, a learning algorithm is used by the neural network to calculate the relationship between input and output which is then utilized to predict output with the entered input values (de Castro et al., 2012). The neural network creates a fitted model in an analytical form, where the parameters are weight, bias, and network typology. Both neural network models, MLP and RBF, are a fully connected multilayer feed-forward supervised learning network trained by the back-propagation algorithm to minimize a quadratic error criterion; no values are fed back to earlier layers. The size of the MLP is described as size of input layer × size of hidden

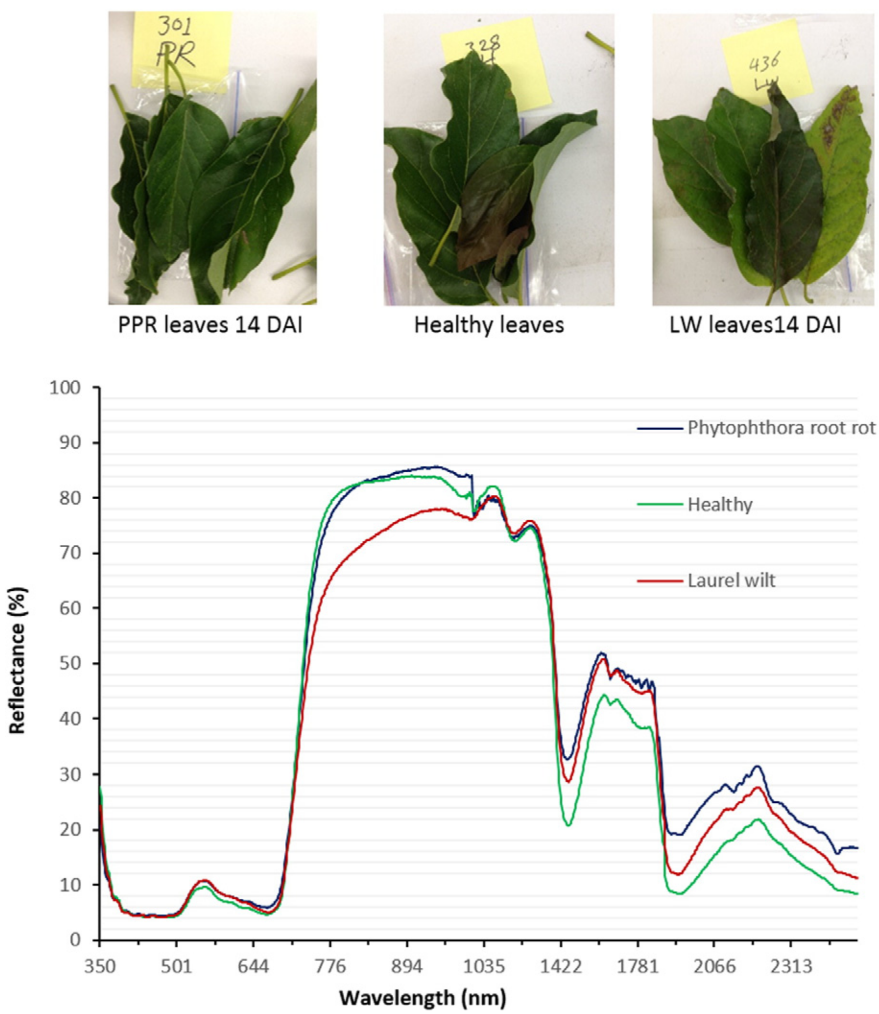

Fig. 1. Visible–near infrared reflectance spectra representing leaves from a healthy tree (H), laurel wilt-inoculated tree (LW) and Phytophthora root rot-inoculated tree (PRR) 14 days after inoculation (DAI).

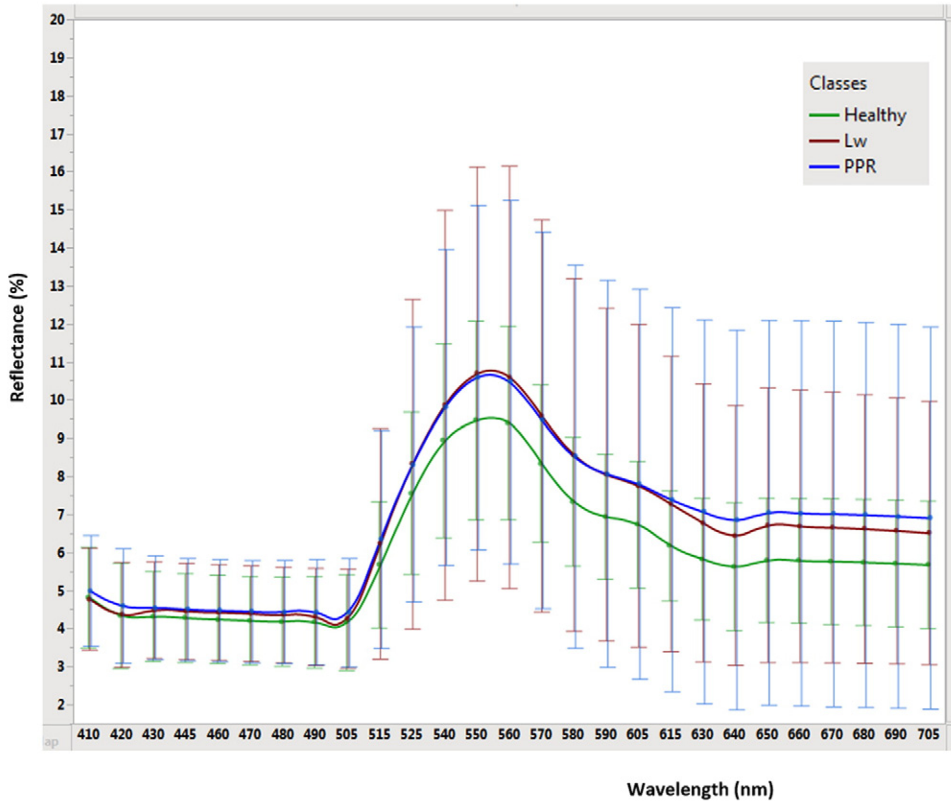

Fig. 2. Standard deviation error bar showing variability in visible reflectance spectra for overlap from healthy leaves (H), laurel wilt-inoculated leaves (LW) and Phytophthora root rot-inoculated leaves (PRR) 14 days after inoculation (DAI).

Fig. 3. Equipment used to take spectral measurements: SVC HR-1024, white panel (Spectralon Reflectance Target) and light source.

layer × size of output layer (Këranen, Aro, Tyystjärvi, & Nevalainen, 2003; Burks, Shearer, Heath, & Donohue, 2005), while RBF is composed by an input layer, a hidden layer, and an output layer (de Castro et al., 2012). The two main differences between these models are that the connections in the RBF between the input and output layers are not weighted, and the transfer functions on the hidden layer nodes are radially symmetric (del Brío & Molina, 2006). A hold-out cross-validation procedure was used to calculate the fitness of MLP and RBF for each classification model. The full dataset was randomly split into three datasets by partitioning the active dataset into training, testing and holdout samples. After learning, the MLP or RBF model was run on the test set that provided an unbiased estimate of the generalization error. SPSS was used to perform spectral analysis (SPSS v.22, 2014, Inc., Chicago; Microsoft Corp., Redmond, WA).

2.2. Part 2: field data—image analysis

After the spectral analysis was carried out at the leaf scale, the study was scaled up to the canopy level, and image analysis was performed in a commercial avocado field to evaluate the camera specifications and flight altitudes for the suitable definition of aerial imagery flight mission.

2.2.1. Study area and image acquisition

For image analysis, filters selected in the previous step were attached to a Tetracam mini-MCA-6 (Tetracam, Inc., CA, USA) multispectral camera with six individual digital sensors arranged in a 3 × 2 array, independent optics and user customizable band pass filters (Andover Corporation, NH, USA). Each unit holds a 1.3 megapixel CMOS sensor (1280 × 1024 pixels), focal length of 9.6 mm and FOV of

$43.7 \times 35.6°$. Images are stored in independent compact flash cards embedded in the camera with 8 bit radiometric resolution.

The MCA camera was used to take multispectral aerial images (Green, G: 580–10 nm; Red, R_{650}: 650–10 nm, Red-edge, $Redge_{740}$: 740–10 nm, Red-edge, $Redge_{750}$: 750–10 nm, NIR, NIR_{760}: 760–10 nm, and NIR, NIR_{850}: 850–40 nm) from a helicopter in February 2014. The multispectral six-band images were taken on a cloudless day in winter (February 17th) of 2014 at sun angles from 10:30 to 12:00 EST and at an off-nadir angle (0–10 from nadir). The images were geo-reference to the world geodesic survey 1984 (WGS84) datum. An avocado field in the CAPA in south Miami-Dade County (latitude and longitude coordinates, 25.593194, −80.423583) with trees at different stages of LW development and H plants was selected (Figs. 4 and 5). This infested field was found during helicopter surveys by LW experts from the Florida Avocado Committee. LW was confirmed in representative trees at all stages of development by recovery of the pathogen on CSMA and confirmation with a diagnostic DNA test (see Carillo et al., 2014), in a rapid action by LW experts from the University of Florida and the Florida Avocado Committee. Three stages of LW development were used to evaluate the disease: 1) early symptoms, in which leaves were still green although had just begun to lose turgidity, developing a slight gray color in some parts; 2) intermediate symptoms, in which leaves began to desiccate, became brittle, wilted, and were a dull gray-green color; 3) late symptoms, in which leaves were completely desiccated, brittle and brown. Every positive LW-infested tree in the field was selected and subsequently used in the image analyses, consisting of 21 infested trees, of which 24% of data corresponded to early stage, 9% to intermediate stage, and 64% to late. A set of 12 healthy trees was used as the control.

The affected portion of the trees as well as healthy control trees were georeferenced and categorized into each degree of development. In addition, geocoordinates for the images were recorded for subsequent ground truthing.

2.2.2. Spatial resolution affected by flight altitude

Images were captured from three altitudes (180, 250 and 300 m) to quantify the influence of image spatial resolution and identify the ideal altitude to detect LW (Fig. 6).

2.2.3. Image pre-processing

Multispectral images were preprocessed for alignment and radiometric correction. Pixel Wrench (PW2) software (Tetracam Inc., Chatsworth, CA, USA) was used to align the six images taken by individual digital sensors in each shoot. A good alignment of all the individual bands is crucial for subsequent image analysis, especially when spectral values of different objects of the image are extracted (Torres-Sánchez et al., 2013). PW2 provides an alignment file that contains information about the translation, rotation, and scaling applied between sensors. A vignetting correction was also carried out in the same process, as recommended by Lebourgeois et al. (2008). The quality of the alignment process was evaluated by using the calibration target data captured in the images at each altitude (Laliberte, Goforth, Steele, & Rango, 2011; Torres-Sánchez et al., 2013). Spatial profiles were taken across the calibration target for different values of the parameter set employed in the PW2, such as the FOV optical calculator and vignette parameters. These spatial profiles consisted of graphics representing the spectral values for each band along a line drawn for both calibration targets in the multiband images using the ENVI image processing software. The best results were used for the alignment process, with displacement among the curves in the spatial profiles for each channel of less than 1 pixel.

For radiometric correction, two calibration targets (each 1.2 m × 1.2 m; Group 8 Technology, Inc., UT, USA) were used during flight. The average reflectance of the black and white targets was 3% and 82%, respectively. An empirical line calibration (Smith & Milton, 1999) was carried out in ENVI software (ENVI, Research Systems Inc., Boulder, CO, USA) to fit digital values of the MCA imagery to the target reflectance spectra (Laliberte et al., 2011; Suárez et al., 2010). Pixels of the images presented digital counts within the range of 0–100% values of reflectance.

2.2.4. Image analysis: spectral resolution affected by flight altitude

Healthy trees and an affected portion of those that showed one of the stages of LW development (early, intermediate and late) were located in the images. Pixel-based retrieved reflectance data of those trees were extracted from images at each of the studied altitudes (180, 250 and 300 m). Only central pixels were selected, avoiding edge pixels and thus, mixed pixels. Mean reflectance spectra calculated for the six spectral bands for each class were used to calculate 28 vegetation

Fig. 4. The selected avocado field with the presence of trees at different stages of laurel wilt infection. This image was captured with a standard RGB camera.

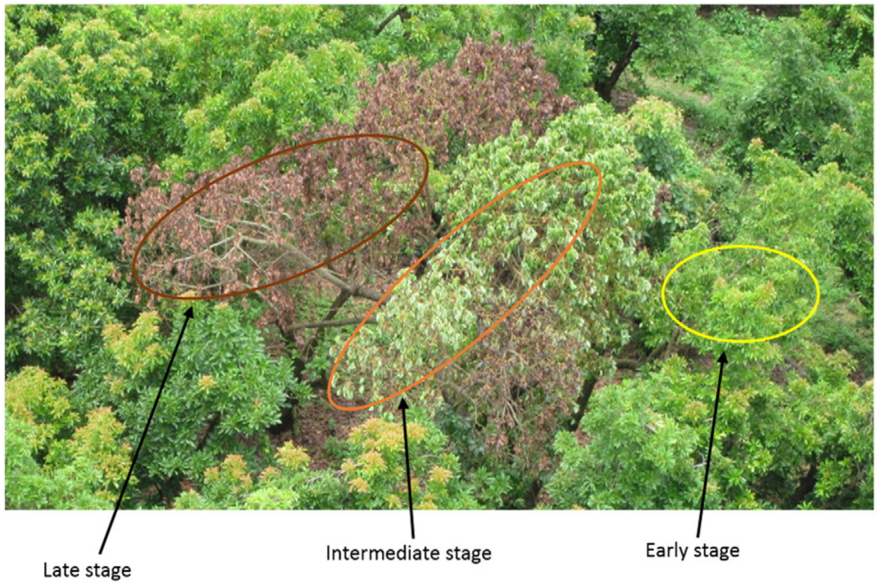

Fig. 5. Three stages of laurel wilt development: early, intermediate and late.

indices (VIs) derived from the six bands of the MCA camera (Table 1). VIs that contained near-infrared (NIR) and/or Red information were applied to possible combinations of the Tetracam bands. The VIs in the present study are related to vegetation conditions and plant structure used elsewhere for agricultural studies (Peña-Barragán, Ngugi, Plant, & Six, 2011; Calderón et al., 2013; Ashourloo, Mobasheri, & Huete, 2014). ENVI software was used to process and analyze the images. To determine the vegetation indices that were useful for separating classes, Tukey's HSD test ($\alpha = 0.01$) was used to analyze VIs (JMP, SAS).

The M-statistic expresses the difference in means of two class histograms normalized by the sum of their standard deviations (σ). The extent to which M-statistics differ will depend on the width of the evaluated histograms. For the same difference in means, wider histograms (larger σ) will cause more overlap and less separation than narrow histograms

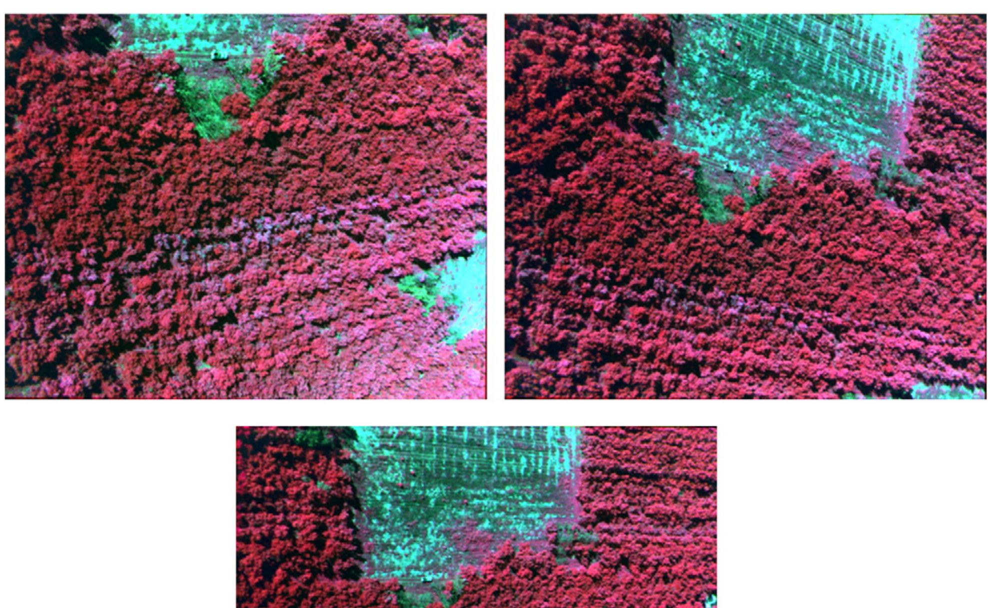

Fig. 6. Images captured with a Tetracam MCA-6 camera at 180 m, 250 m and 300 m above the field.

Table 1
Vegetation indices explored in this study derived from the six bands of the MCA camera.

Vegetation index	VI adapted to laurel wilt detection bands	Adapted from reference
R/G	R_{650}/G; $Redge_x/G$;	–
NIR/G	NIR_y/G;	–
Red-G	$R_{650}-G$; $Redge_x-G$	De Castro et al. (2015)
Red-edge/R band ratios	$Redge_x/R_{650}$	This study
Redged/Redged	$Redge_{750}/Redge_{740}$	This study
Green vegetation index	$VIGreen = \frac{G-R^*}{G+R^*}$	Gitelson et al. (2002)
Green NDVI	$GNDVI = \frac{NIR_y-G}{NIR_y+G}$	Gitelson and Merzlyak (1996)
Normalized Difference Vegetation Index	$NDVI = \frac{NIR^*-R^*}{NIR^*+R^*}$	Rouse, Haas, Schell, and Deering (1973)
Excess Red	$ExR = 1.4R^* - G$	Meyer, Hindman, and Lakshmi (1998)
Modified Excess Red	$MExR = 1.4NIR_x - G$	This study
Ratio Vegetation Index	$RVI = \frac{NIR_y}{R^*}$	Jordan (1969)
Difference Vegetation Index	$DVI = NIR^* - R^*$	Jordan (1969)
Modified Simple Ratio	$MSR = \frac{\left(NIR_y/R^*\right)-1}{\left(NIR_y/R^*\right)^{0.5}+1}$	Chen (1996)
Triangular Veg. Index	$TVI = 0.5*[120(NIR_y - R^*) - 200(R^* - G)]$	Broge and Leblanc (2000)
Modified Triangular Vegetation Index 1	$MTVI_1 = 1.2*[1.2(NIR_y - G) - 2.5(R^* - G)]$	Haboudane, Miller, Pattey, Zarco-Tejada, and Strachan (2004)
Modified Triangular Vegetation Index 1	$MTVI_2 = \frac{1.5*[1.2(NIR_y-G)-2.5(R^*-G)]}{\sqrt{(2*NIR_y+1)^2-(6*NIR_y-5*\sqrt{R^*})}-0.5}$	Haboudane et al. (2004)
Renormalized Difference Vegetation Index	$RDVI = (NIR_y-R^*)/\sqrt{(NIR_y+R^*)}$	Rougean and Breon (1995)
Improved SAVI with self-adjustment factor L	$MASAVI = 0.5*\left[2*NIR_y+1-\sqrt{(2*NIR_y+1)^2-8*(NIR_y-R^*)}\right]$	Qi, Chehbouni, Huete, Keer, and Sorooshian (1994)
Optimized Soil-Adjusted Vegetation Index	$OSAVI = 1.16*\frac{(NIR_y-R^*)}{(NIR_y+R^*+0.16)}$	Rondeaux, Steven, and Baret (1996)
Modified CARI	$MCARI = [(NIR_y-R^*)-0.2(NIR_y-G)]*\left(NIR_y/R^*\right)$	Daughtry, Walthall, Kim, Brown de Colstoun, and McMurtrey (2000)
Transformed CARI	$TCARI = 3*[(NIR_y-R^*)-0.2*(NIR_y-G)]*\left(NIR_y/R^*\right)$	Haboudane, Miller, Tremblay, Zarco-Tejada, and Dextraze (2002)
Modified CARI 1	$MCARI_1 = 1.2*[2.5*(NIR^* - R^*) - 1.3*(NIR^* - G)]$	Haboudane et al. (2004)
Modified CARI 2	$MCARI_2 = \frac{1.5*[2.5*(NIR_y-R^*)-1.3*(NIR_y-G)]}{\sqrt{(2*NIR_y+1)^2-(6*NIR_y-5*\sqrt{R^*})}-0.5}$	Haboudane et al. (2004)
Modified Vogelmann Indices for laurel wilt detection bands	$VOG_1 = \frac{Redged_{750}-NIR_{760}}{R_{650}+Redged_{740}}$	This study
	$VOG_2 = \frac{NIR_{760}-NIR_{850}}{Redged_{740}+Redged_{750}}$	
	$VOG_3 = \frac{NIR_{760}-NIR_{850}}{R_{650}+Redged_{750}}$	
NIR, Red-edge and Green Combination Index	$NRGCI = \frac{NIR_{760}-Redged_{750}}{G_{580}}$	This study
NIR, Red-edge and Red Combination Index	$NRRCI = \frac{NIR_{760}-Redged_{750}}{R_{650}}$	This study
NIR and Red-edge Combination Index	$NRCI = \frac{NIR_{760}-Redged_{750}}{Redged_{740}}$	This study
Red-Edge Vegetation Stress Index	$RVSI_1 = \frac{R_{650}+Redged_{750}}{2} - Redged_{740}$	Merton and Huntington (1999)
	$RVSI_2 = \frac{R_{650}+NIR_{750}}{2} - Redged_{750}$	

$G = G_{580}$. NIR_y in the form represents the specific MCA-camera band (760 and 850 nm bands) used to calculate the VI. R^* in the form represents the specific MCA-camera band (R_{650}; $Redge_{740}$; $Redge_{750}$) used to calculate the VI. $Redege_x$ in the form represents the specific MCA-camera band (740 and 750 nm bands) used to calculate the VI.
CARI: Chlorophyll Absorption in Reflectance Index.

(smaller σ) (Kaufman & Remer, 1994). The M-statistic was used to establish the best vegetation indices for the discrimination, where M < 1.0 indicates poor separation, M > 1.0 indicates good separation, and better separation occurs for larger M values (Smith et al., 2007).

$$M = \frac{\mu_a - \mu_b}{\sigma_a + \sigma_b}$$

2.2.5. Grouping data

The analyses were conducted taking into account 2-class or 4-class systems. The 2-class system was designed to differentiate H and LW trees which is sufficient to identify affected trees for removal, whereas the 4-class system was used to differentiate H plants and the three stages of LW development, allowing for management depending on stage development.

3. Results and discussion

3.1. Part 1: spectral analysis—band selected

There were significant differences among H, LW and PRR plants in the red-edge (740 and 750) and NIR (760, 940, and 950) regions (Table 2). At 580 nm (green region) it was possible to discriminate H plants from those affected by either disease. Furthermore, significant differences in spectral data between the LW plants and the other classes were observed in some wavelengths of the red region (720 and 730 nm) and most of the NIR region. These results documented sufficient spectral differences among H, LW and PRR plants at 14 DAI for correct classification, and indicated the spectral regions to examine for LW detection.

Table 3 shows the classification results obtained from the multilayer perceptron neural network using different sets of parameters reflecting training, testing and holdout samples. The results obtained with MLP were better than those achieved with RBF (data not shown) with correct classification percentages ranging from 91% to 100% in all datasets (Table 3). The most frequently selected 10 nm-wavelengths were found in the red-edge and near-infrared parts of the spectrum. The 760, 750, and 740 nm wavelengths were always selected by the MLP neural network for the different parameter sets, indicating that these wavelengths are crucial for correctly classifying leaves from H, LW and PRR plants. Other wavelengths (830 and 950 nm) were selected in the NIR region for some of the neural networks, while wavebands lower than 700 nm were never chosen.

The most effective wavelengths identified by MLP neural network (760, 750, and 740 nm at a 10-nm bandwidth) and ANOVA analysis were selected for use with the MCA-6 camera. An additional filter was

Table 2
Spectral 10 nm-wavelengths mean values for healthy, laurel wilt-inoculated plants and Phytophthora root rot inoculated plants.

Classes	10 nm-wavelengths[a]																						
	580	720	730	740	750	760	770	780	795	810	820	830	840	850	860	875	885	895	910	920	930	940	950
Healthy	7.3 b	31.2 a	46.2 a	59.8 a	69.2 a	74.8 a	78.2 a	80.1 a	81.2 a	81.9 a	82.4 a	82.8 a	83.0 a	83.1 a	83.3 a	83.5 a	83.8 a	83.9 a	83.9 a	83.8 a	83.8 a	83.4 b	82.2 b
Lw	8.6 a	28.4 b	39.4 b	49.2 c	56.4 c	71.6 c	64.3 b	66.5 b	68.2 b	69.5 b	70.7 b	71.8 b	72.7 b	73.6 b	74.3 b	75.3 b	76.1 b	76.6 b	77.2 b	77.6 b	77.9 b	77.9 c	77.7 c
PPR	8.5 a	31.2 a	44.4 a	56.5 b	65.7 b	71.6 b	75.6 a	78.1 a	79.8 a	81.1 a	82.1 a	82.9 a	83.3 a	83.7 a	83.9 a	84.4 a	84.7 a	85.0 a	85.3 a	85.5 a	85.5 a	85.4 a	84.9 a

Abbreviations: Lw: Laurel wilt infested plants; PPR: Phytophthora root rot plants.
For each column and classes mean values followed by the same letter are not statistically different at $p = 0.01$.
[a] Only some statistically different wavelengths are shown.

Table 3
Multispectral classification for 10-nm bandwidth data for healthy, laurel wilt-inoculated plants and Phytophthora root rot inoculated plants using MLP neural networks according to several parameter sets.

Parameter set[a]	Importance of variables	Hidden layer	Neurons of hidden layer	Overall classification
7–2–1	**760, 750, 740**, 950	1	5	91.0%
6–2–2	**750, 740, 760**	1	7	95.8%
6–3–1	**740, 760, 750**, 950	1	7	91.5%
8–1–1	**740, 750**, 830, **760**	1	9	100%

MLP: multilayer perceptron.
The values given in bold represent the common wavelengths selected in all MLP neural networks.
[a] Parameter set: sample partitioning into training–testing-holdout.

selected in the red region (650 nm) because most of the VIs rely on some combination of NIR and red reflectance (Jordan, 1969). Increase in leaf area index corresponds with an increase in chlorophyll absorption and NIR-scattering and decreases with exposed substrate, resulting in decreasing red and increasing NIR reflectance (Thenkabail, Lyion, & Huete, 2012). A filter in the green region was used taking into account subtle changes that occur with an increase in leaf area index, including increased green reflectance (Gitelson, Kaufman, & Rundquist, 2002). ANOVA analysis (Table 2) indicated that a 580–10 nm filter was the most effective wavelength in the green region to distinguish H from LW and PRR plants. The last filter was for the NIR region in which more differences were found among the test plants (Fig. 1), making a narrow filter unnecessary. Therefore, for economic reasons, a 40 nm bandwidth at 850 nm was chosen, the wavelength that was selected by the MLP neural network.

3.2. Part 2: image analysis

3.2.1. Effect of flight altitude

Flight altitude is an important parameter to take into account when acquiring remote images, since it has strong implications in spatial resolution, flight duration, area covered by each image, time-consumption, image processing, spectral resolution and cost. The higher the spatial resolution, the finer the details that can be discriminated in the image. However, when images are taken at low altitude to increase spatial resolution, more time is needed to capture the entire area of work (Gómez-Candón, De Castro, & López-Granados, 2014), increasing flight time and cost. In addition, at a lower altitude, the number of images needed to cover the whole field increases, so a mosaicking process may be needed (Torres-Sánchez et al., 2013).

As a result of the spectral analysis and band selection, the MCA-6 Tetracam camera was upgraded with the following filters: 580–10 nm, 650–10 nm, 740–10 nm, 750–10 nm, 760–10 nm and 850–40 nm. It was used at different flight altitudes to quantify the influence of image spatial resolution in detecting LW (Fig. 6). The imagery pixel size was directly proportional to the flight altitude, with pixel sizes of 11.5 cm at 180 m, 15.3 cm at 250 m and 19.1 cm at 300 m.

Avocado orchards vary in size from 0.04 to 202 ha (USDA, 2009). Orchards larger than 6 ha are rare and most are between 0.4 and 2 ha (Evans & Bernal Lozano, 2015). The area covered by images taken at the evaluated altitudes increased from 1.7 ha at 180 m to 4.8 ha at 300 m. Therefore, to minimize flight and image analysis duration the most effective altitudes would be 250 m and 300 m, with an area covered of 3 ha and 4.8 ha, respectively. Lowering the altitude to 180 m in a large field required a mosaicking process to stitch the images together.

The optimum pixel size to discriminate H and LW trees is related to tree canopy size. Since an average mature avocado tree canopy is 7–9 m in diameter, any of the tested altitudes would be able to discriminate an LW tree.

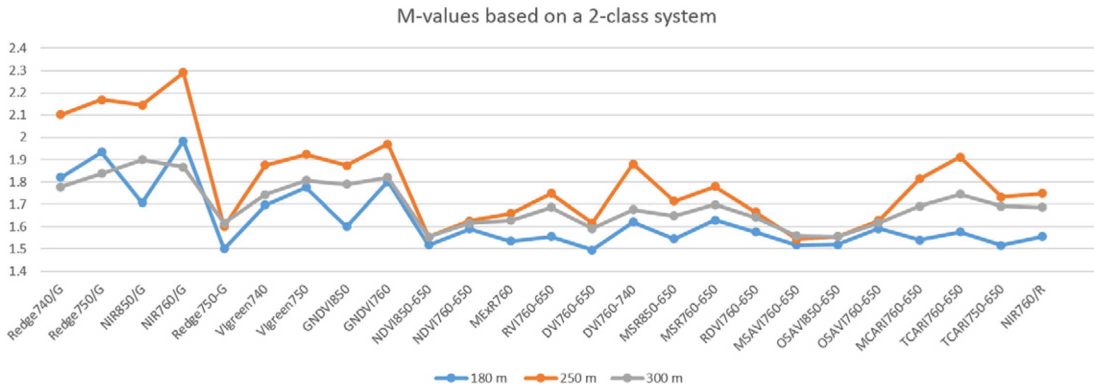

Fig. 7. Best vegetation indices according to M-values (>1.5) obtained in the 2-class system separation, among healthy plants and laurel wilt-affected trees, as affected by flight altitude.

3.2.2. Vegetation indices and optimum number of classes

Reflectance values captured at each flight altitude for H and LW trees were studied based on a 2-class and a 4-class system with VIs.

3.2.2.1. System based on a 2-class system: healthy plants and laurel wilt-infested trees. Using the 2-class system, significant differences in spectral data between H and LW trees were observed in most of the VIs at all altitudes (data not shown). The M-statistic results quantified the separation between H and LW plants, and showed the best indices to discriminate both classes. M values varied according to the flight altitude and vegetation indices, achieving values >1.0 in most cases. These results indicate good separation and satisfactory results for vegetation classification (Smith et al., 2007). Fig. 7 shows the best results obtained for M-values using a 2-class system as affected by flight altitude. Twenty-five VIs achieved an M-value higher than 1.5 in all altitudes showing to have high discriminatory power (Smith et al., 2007). The best M-values were obtained at 250 m, and second best at 300 m.

NIR_{750}/G performed significantly better than other indices at 180, 250 and 300 m, with the next best discriminator being the $Redge_{750}$/G, followed by the NIR_{850}/G; $Redge_{740}$/G; $GNDVI_{760}$; $VIGreen_{750-650}$; $DVI_{760-740}$; $VIGreen_{740}$; and $TCARI_{750-650}$; $GNDVI_{850}$.

With the 2-class system and aerial images taken by the upgraded MCA-6 camera H and LW trees could be efficiently discriminated at different altitudes, and VIs were identified to develop an LW classification algorithm. Those VIs were designed to measure structural and color

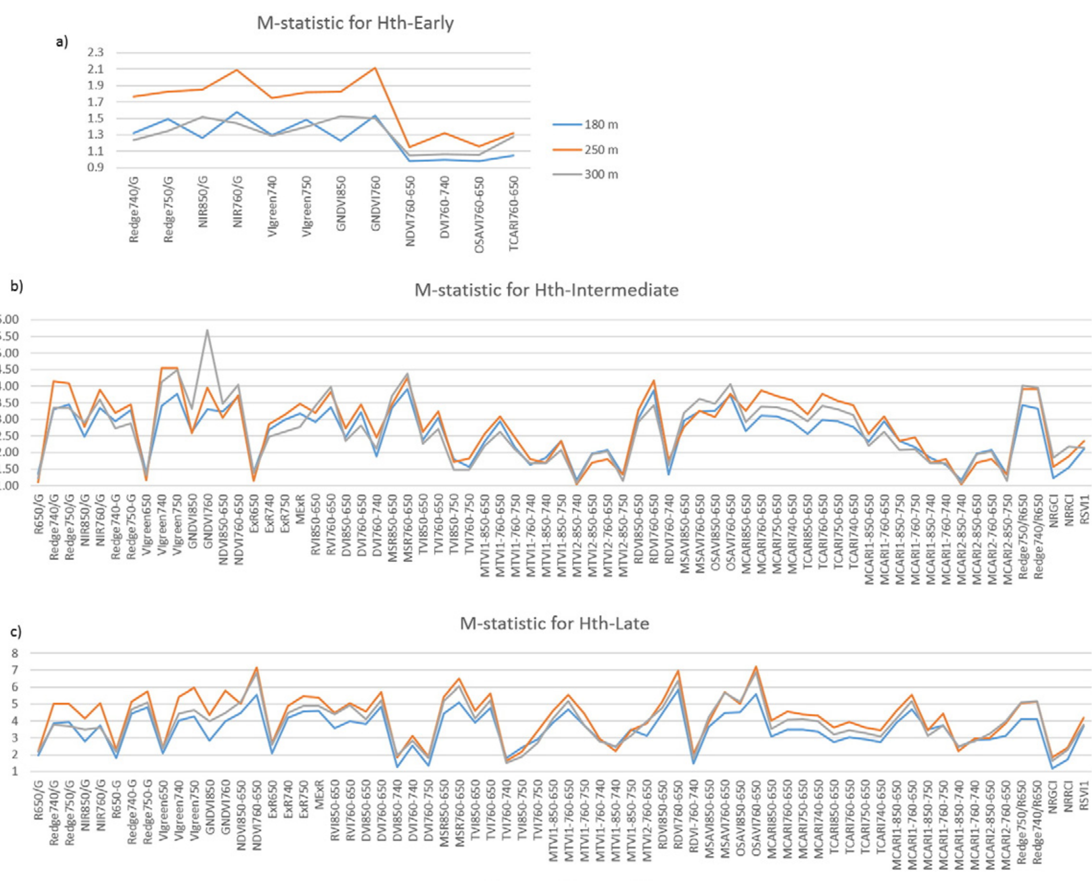

Fig. 8. M-values for best vegetation indices, according to M-values >1.0, obtained in the 4-class discrimination system as affected by flight altitude: a) healthy and early stage separation, b) healthy and intermediate stage separation, and c) healthy and late stage separation.

changes in the vegetation properties. When the tree is infested with LW, the amount of chlorophyll in the leaves is reduced and the cell structure is damaged, since this disease plugs the xylem impeding the flow of water and nutrients in affected trees, resulting in an increase in tree temperature (De Castro et al., 2015).

3.2.2.2. Development of a 4-class system. In the 4-class system, spectral data from H plants were compared with those from early, intermediate and late stages of LW development. Distinction of different LW development stages was not studied, since the objective was to detect LW trees and discriminate these from H trees. Significant differences in spectral data were observed between H and each of the LW stages when analyzed at 180, 250 and 300 m (data not shown). Therefore, this system could be used to detect LW at each developmental stage using aerial images taken by the selected filters.

The M-statistic was calculated for each of the VIs at three flight altitudes. Only M values >1.0 were considered for this study (Fig. 8) since lower values have been shown to provide a poor spectral separation between H and LW trees (de Castro et al., 2015). M results varied according to the disease development stage and altitude. Regardless of the acquisition altitude, a high number of VIs had M values >1.0 when late or intermediate stage classes were compared to H trees, reaching these VIs with greater M-values than those obtained in the comparison between H and early stage of LW development.

In general, H plants could be distinguished from LW plants best during the late stage of development (Fig. 8c), as the M-statistic was >5 in many cases indicating robust separation of these classes (Torres-Sánchez et al., 2013). Good separation was also achieved between H plants and those at the intermediate stage of development (Fig. 8b), as a large number of VIs had high M-values. Although H and late or intermediate stage LW plants could be distinguished with a large number of VIs, it was more difficult to separate H from early stage LW trees. In the intermediate and late stage of development, external symptoms have developed, and leaves became wilted or desiccated and were a dull gray-green or brown color, while leaves in early stage were still green, and just beginning to lose turgidity.

Twelve VIs had M values higher than 1.0 when H trees were compared to early stage trees. In the first stage of disease development, internal symptoms began soon after infestation because the xylem function is impaired and hydraulic conductivity is reduced; however very slight symptoms can be discerned in the infested tree (Ploetz et al., 2013). Thus, pixel-based retrieved reflectance spectra of early stage trees were similar in the visible region to H data that showed leaves vigorous in green color (Fig. 5). These results agree with spectral information obtained under control for LW leaves 14 DAI (Fig. 1). Early LW stage must be identified by detecting differences in spectral data resulting from the cell structure, which were found in ratios between the NIR and red-edge region, as shown in Fig. 8a. Thus, LW trees even with minimal symptoms could be distinguished using aerial images taken with the selected filters.

With regard to the flight altitude, the magnitude of M-statistic for most of VIs was greatest at 250 m for all the scenarios. M-results were similar for both 180 and 300 m altitudes. These results agree with those obtained in the analyses based on a 2-class system (Fig. 7) and offer high robustness in the discrimination of laurel wilt disease at this altitude. A preliminary conclusion could be that the most effective altitude to take images for LW detection is 250 m. Moreover, images taken at that altitude cover the whole field area for most of the avocado orchards in Florida (0.4–2 ha) minimizing flight and image analyses duration. The pixel size for 250 m altitude images (15.3 cm) is also able to discriminate the mature avocado tree canopy.

3.2.2.3. Vegetation indices. As a general statement, the VIs that best performed, regardless of class-altitude combination, were $TCARI_{760–650}$ as well as GNDVI, NIR/G, Redge/G, and VIGreen using any of the bands related to Red-edge (740 and 750 nm) and NIR (760 and 850 nm) regions. These VIs showed robustness in the ability of discriminating LW at each of development stages, even with minimal external symptoms. Therefore, these VIs should be used to develop an LW classification algorithm in further research.

3.2.2.4. Optimum number of classes. Focusing on the ultimate objective of developing a LW classification algorithm, it is necessary to establish the effective number of classes. The results obtained herein reported on the utility of the 2-class and 4-class systems to classify LW using aerial images and the aforementioned VIs. Fig. 9 shows the M values reached with those VIs as affected by class aggrupation and flight altitude. In all cases, the best discriminatory power was reached for the separation late stage-H, followed by the separation intermediate stage-H, as explained above. However, no large differences in M-values were found between the H-early stage separation and the H-LW (2-class system) separation, showing similar separation capacity. According to our findings, any of both systems would allow identifying LW infested trees using the selected VIs and filters. However, it should be more convenient to develop the classification algorithm based on four classes (H, early, intermediate and late), as the high capacity to separate late and intermediate stage from H will make it more accurate (Fig. 9).

The most important achievement of this research was the successful identification of LW, even with minimal symptoms, using six-band aerial images. The more efficient wavebands to separate H and early stage of LW development were selected and the corresponding filters were attached to the MCA-6 camera. The ideal flight altitude, number of classes, and VIs for detecting LW using aerial images were determined, satisfying the overall research objective.

The early detection of LW will facilitate implementation of management strategies to prevent the development and spread of the disease. A classification algorithm based on a 4-class system could be used to apply site-specific control tactics depending on the developmental stage of the disease. By using remote sensing techniques, such as a properly selected filter for the MCA-6 camera, and discrimination algorithms to identify early stage of LW development trees could help farmers control the movement of this devastating disease and keep the Florida CAPA the second leading avocado producer in the nation.

4. Conclusions

As part of an overall research program to detect and suppress LW in Florida's CAPA, the spatial and spectral requirements for quick and accurate detection of LW were evaluated in this study. Spectral data analyses showed significant differences among H, LW and PRR plants. The most effective wavelengths were identified by MLP neural network, which achieved nearly 100% and 100% correct classifications, and the filters were updated to a MCA-6 Tetracam camera (580–10 nm, 650–10 nm, 740–10 nm, 750–10 nm, 760–10 nm and 850–40 nm).

Aerial image analysis proved the utility of the selected filters for successful identification of LW, even trees in early stage of disease development with minimal symptoms. The effect of flight altitude was evaluated due to its strong implications in spatial resolution, flight and image analysis duration. The ideal flight altitude of 250 m, corresponding to a pixel size of 15.3 cm, was selected according to the magnitude of M-values and biological parameters such as canopy size and orchard size. Satisfactory results were also achieved at 180 and 300 m.

Optimum VIs were identified to develop an LW classification algorithm, as determined by higher M values: $TCARI_{760–650}$ as well as GNDVI, NIR/G, Redge/G and VIGreen using any of the bands related to Redge (740 and 750 nm) or NIR regions (760 and 850 nm). Regarding the most efficient number of classes to perform the algorithm, results reported on the utility of the 2-class and 4-class systems using the aforementioned VIs. However, according to the findings, it should be more convenient to develop the algorithm based on a 4-class system (H, early, intermediate and late), since higher accuracy could be reached in the classification map versus the 2-class system.

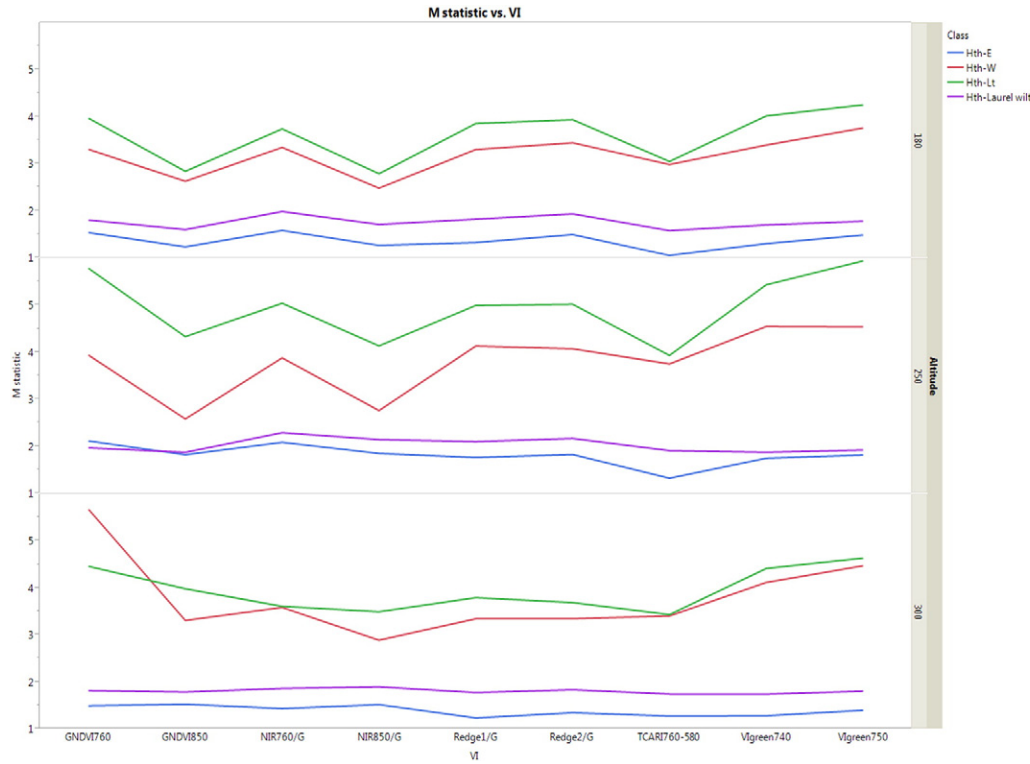

Fig. 9. M-values for the effective vegetation indices obtained in the 2-class and 4-class discrimination systems as affected by flight altitude. The *Hth-laurel wilt* class represents the 2-class system, while *Hth-E*, *Hth-W* and *Hth-Lt* represent the 4-class system used to differentiate healthy plants and each of three infestation stages of laurel wilt individually (early, intermediate and late).

Use of the MCA-6 camera upgraded with the selected filters will enable a rapid and accurate assessment of laurel wilt disease progression, as well as provide a valuable tool for mitigating this important threat to Florida's avocado production. The authors suggest developing the algorithm in further research for a method of quick and accurate early detection of LW. An algorithm based on a 4-class system would be able to detect different stages of laurel wilt progress and could be used to apply site-specific control tactics depending on the stage.

The importance of avocado is recognized throughout the world, making it necessary to prevent the spread of this disease. The use of early detection techniques through methodology proposed in this research could potentially allow farmers to control the movement of this disease through proper management strategies, as without a reliable control strategy the cost to replace avocado trees destroyed by this disease in Florida would be about $423 million.

Acknowledgements

The authors thank the Florida Department of Agriculture and Consumer Services, USDA Specialty Block Grant No. 019730 for funding this investigation. The authors thank Don Pybas, Sherrie Buchanon and Josh Konkol for their very useful help.

References

Ashourloo, D., Mobasheri, M.R., & Huete, A. (2014). Evaluating the effect of different wheat rust disease symptoms on vegetation indices using hyperspectral measurements. *Remote Sensing*, *6*, 5107–5123.

Broge, N.H., & Leblanc, E. (2000). Comparing prediction power and stability of broadband and hyperspectral vegetation indices for estimation of green leaf area index and canopy chlorophyll density. *Remote Sensing of Environment*, *76*, 156–172.

Burks, T.F., Shearer, S.A., Heath, J.R., & Donohue, K.D. (2005). Evaluation of neural-network classifiers for weed species discrimination. *Biosystems Engineering*, *91*(3), 293–304.

Calderón, R., Navas-Cortés, J.A., Lucena, C., & Zarco-Tejada, P.J. (2013). High-resolution airborne hyperspectral and thermal imagery for early detection of *Verticillium* wilt of olive using fluorescence, temperature and narrow-band spectral indices. *Remote Sensing of Environment*, *139*, 231–245.

Carillo, D., Duncan, R.E., Ploetz, J.N., Campbell, A.F., Ploetz, R.C., & Peña, J.E. (2014). Lateral transfer of a phytopathogentic symbiont among native and exotic ambrosia beetles. *Plant Pathology*, *63*, 54–62.

Chemically Speaking Newsletter (2009, February). *Pesticide Potpourri*. Gainesville: University of Florida, IFAS Ext. Pesticide Information Office, 6 (http://pested.ifas.ufl.edu/newsletter.html. Accessed 9 January 2015).

Chen, J. (1996). Evaluation of vegetation indices and modified simple ratio for boreal applications. *Canadian Journal of Remote Sensing*, *22*, 229–242.

Dammer, K.H., Möller, B., Rodemann, B., & Heppner, D. (2011). Detection of head blight (*Fusarium* ssp.) in winter wheat by color and multispectral image analyses. *Crop Protection*, *30*, 420–428.

Daughtry, C.S.T., Walthall, C.L., Kim, M.S., Brown de Colstoun, E., & McMurtrey, J.E., III (2000). Estimating corn leaf chlorophyll concentration from leaf and canopy reflectance. *Remote Sensing of Environment*, *74*, 229–239.

De Castro, A.I., Ehsani, R., Ploetz, R.C., Crane, J.H., & Buchanon, S. (2015). Detection of laurel wilt disease in avocado using low altitude aerial imaging. *PLoS ONE*, *10*(4), e0124642. http://dx.doi.org/10.1371/journal.pone.0124642.

De Castro, I.A., Jurado-Expósito, M., Peña-Barragán, J.M., & López-Granados, F. (2012). Applying neural networks to hyperspectral and multispectral field data for discrimination of cruciferous weeds in winter crops. *The Scientific World Journal*, 630390 (section Agronomy).

Del Brío, M.B., & Molina, S.A. (2006). *Redes neuronales y sistemas borrosos* ((3rd Ed.)). Madrid, Spain: RA-MA.

Du, Q., Chang, N.B., Yang, C., & Srilakshmid, K.R. (2008). Combination of multispectral remote sensing, variable rate technology and environmental modeling for citrus pest management. *Journal of Environmental Management*, *86*, 14–26.

Estep, L., Terrie, G., & Davis, B. (2004). Technical note: Crop stress detection using AVIRIS hyperspectral imagery and artificial neural networks. *International Journal of Remote Sensing*, *25*, 4999–5004. http://dx.doi.org/10.1080/01431160412331291242.

Evans, E.A., & Crane, J.H. (2012). Estimates of the replacement costs of commercial and backyard avocado trees in South Florida. *Electronic data information source (EDIS) FE82500*. Gainesville, FL: Food and Resource Economics Department, University of Florida (http://edis.ifas.ufl.edu/pdffiles/FE/FE82500.pdf. Accessed 9 January 2015).

Evans, E.A., & Bernal Lozano, I. (2015). Sample avocado production costs and profitability analysis for Florida. *Electronic data information source (EDIS) FE837*. Gainesville, FL: Food and Resource Economics Department, University of Florida (http://edis.ifas.ufl.edu/pdffiles/FE/FE83700.pdf. Accessed 19 March 2015).

Evans, E.A., Crane, J.H., Hodges, A., & Osborne, J.L. (2010). Potential economic impact of laurel wilt disease on the Florida avocado industry. *HortTechnology*, *20*, 234–238.

FAO (2010). FAOSTAT. online database at: http://www.fao.org/default.htm (Accessed 9 January 2015)

Flinn, A. (2014) Personal communication. Manager of Avocado Administrative Committee. Homestead, FL (October 30).

Fraedrich, S.W., Harrington, T.C., Rabaglia, R.J., Mayfield, A.E., Hanula, J.L., Eickwort, J.M., & Miller, D.R. (2008). A fungal symbiont of the redbay ambrosia beetle causes a lethal wilt in redbay and other Lauraceae in the Southeastern United States. *Plant Disease*, *92*, 215–224.

García-Ruiz, F., Sankaran, S., Maja, J.M., Lee, W.S., Rasmussen, J., & Ehsani, R. (2013). Comparison of two aerial imaging platforms for identification of Huanglongbing-infected citrus trees. *Computers and Electronics in Agriculture*, *91*, 106–115.

Gitelson, A.A., & Merzlyak, M.N. (1996). Signature analysis of leaf reflectance spectra: Algorithm development for remote sensing of chlorophyll. *Journal of Plant Physiology*, *148*, 494–500.

Gitelson, A.A., Kaufman, Y.J., Stark, R., & Rundquist, D. (2002). Novel algorithms for remote estimation of vegetation fraction. *Remote Sensing of Environment*, *80*, 76–87.

Gómez-Candón, D., De Castro, A.I., & López-Granados, F. (2014). Assessing the accuracy of mosaics from unmanned aerial vehicle (UAV) imagery for precision agriculture purposes in wheat. *Precision Agriculture*, *15*, 44–56.

Gray, C.J., Shaw, D.R., Gerard, P.D., & Bruce, L.M. (2008). Utility of multispectral imagery for soybean and weed species differentiation. *Weed Technology*, *22*(4), 713–718.

Haboudane, D., Miller, J.R., Pattey, E., Zarco-Tejada, P.J., & Strachan, I. (2004). Hyperspectral vegetation indices and novel algorithms for predicting green LAI of crop canopies: Modeling and validation in the context of precision agriculture. *Remote Sensing of Environment*, *90*, 337–352.

Haboudane, D., Miller, J.R., Tremblay, N., Zarco-Tejada, P.J., & Dextraze, L. (2002). Integration of hyperspectral vegetation indices for prediction of crop chlorophyll content for application to precision agriculture. *Remote Sensing of Environment*, *81*, 416–426.

Han, J., Kamner, M., & Pei, J. (2012). *Data mining. Concepts and techniques* (3rd ed.). Waltham, MA, USA: Morgan Kaufmann Publishers, Elsevier Inc.

Harrington, T.C., Fraedrich, S.W., & Aghayeva, D. (2008). *Raffaelea lauricola*, a new ambrosia beetle symbiont and pathogen on the Lauraceae. *Mycotaxon*, *102*, 399–404.

Heremans, S., Bossyns, B., Eerens, H., & Van Orshoven, J. (2011). Efficient collection of training data for sub-pixel land cover classification using neural networks. *International Journal of Applied Earth Observation and Geoinformation*, *13(4)*. (pp. 657–667). Elsevier B.V.

Inch, S.A., & Ploetz, R.C. (2012). Impact of laurel wilt, caused by *Raffaelea lauricola*, on xylem function in avocado, *Persea americana*. *Forest Pathology*, *42*, 239–245.

Jordan, C.F. (1969). Derivation of leaf area index from quality of light on the forest floor. *Ecology*, *50*, 663–666.

Kaufman, Y.J., & Remer, L.A. (1994). Detection of forests using mid-IR reflectance: An application for aerosol studies. *IEEE Transactions on Geoscience and Remote Sensing*, *32*, 672–683.

Kĕranen, M., Aro, E.M., Tyystjärvi, E., & Nevalainen, O. (2003). Automatic plant identification with chlorophyll fluorescence fingerprinting. *Precision Agriculture*, *4*, 53–67.

Laliberte, A.S., Goforth, M.A., Steele, C.M., & Rango, A. (2011). Multispectral remote sensing from unmanned aircraft: Image processing workflows and applications for rangeland environments. *Remote Sensing*, *3*(11), 2529–2551.

Lebourgeois, V., Bégué, A., Labbé, S., Mallavan, B., Prévot, L., & Roux, B. (2008). Can commercial digital cameras be used as multispectral sensors? A crop monitoring test. *Sensors*, *8*(11), 7300–7322.

López-Granados, F. (2011). Weed detection for site-specific weed management: mapping and real-time approaches. *Weed Research*, *51*, 1–11.

Merton, R., & Huntington, J. (1999). Early simulation of the ARIES-1 satellite sensor for multi-temporal vegetation research derived from AVIRIS. *Summaries of the Eighth Annual JPL Airborne Earth Science Workshop* (pp. 299–307). Pasandena, CA, USA: Jet Propulsion Laboratory, National Aeronautics and Space Administration.

Meyer, G.E., Hindman, T.W., & Lakshmi, K. (1998). Machine vision detection parameters for plant species identification. *The SPIE Proceedings*, *Vol. 3543*, (Bellingham, WA).

Naidu, R.A., Perry, E.M., Pierce, F.J., & Mekuria, T. (2009). The potential of spectral reflectance technique for the detection of grapevine leafroll-associated virus-3 in two red-berried wine grape cultivars. *Computers and Electronics in Agriculture*, *66*, 38–45.

Peña-Barragán, J.M., Ngugi, M.K., Plant, R.E., & Six, J. (2011). Object-based crop identification using multiple vegetation indices, textural features and crop phenology. *Remote Sensing of Environment*, *115*, 1301–1316.

Ploetz, R.C., & Carrillo, D. (2015). Laurel wilt of avocado: Epidemiology and management of a recalcitrant disease of an important crop. *Journal of Phytopathology* (in press).

Ploetz, R.C., Harrington, T., Hulcr, J., Fraedrich, S., Smith, J.A., Inch, S., Kendra, P., Mayfield, A.E., et al. (2011a). Recovery plan for laurel wilt of avocado (caused by *Raffaelea lauricola*). *National Plant Disease Recovery System. Homeland Security Presidential Directive Number 9 (HSPD-9)* (Available: http://www.ars.usda.gov/research/docs.htm?docid=14271).

Ploetz, R.C., Hulcr, J., Wingfield, M., & de Beer, Z.W. (2013). Destructive tree diseases associated with ambrosia and bark beetles: Black swan events in tree pathology? *Plant Disease*, *95*, 856–872.

Ploetz, R.C., Pérez-Martínez, J.M., Smith, J.A., Hughes, M., Dreaden, T.J., Inch, S.A., & Fu, Y. (2012). Responses of avocado to laurel wilt, caused by *Raffaelea lauricola*. *Plant Pathology*, *61*, 801–808.

Ploetz, R.C., Peña, J.E., Smith, J.A., Dreaden, T.L., Crane, J.H., Schubert, T., & Dixon, W. (2011b). Laurel wilt is confirmed in Miami-Dade County, center of Florida's commercial avocado production. *Plant Disease*, *95*, 1599.

Pozdnyakova, L., Oudemans, P.V., Hughes, M.G., & Giménez, D. (2012). Estimation of spatial and spectral properties of phytophthora root rot and its effects on cranberry yield. *Computers and Electronics in Agriculture*, *37*, 57–70.

Pybas, D. (2009). Personal communication, Miami, FL.

Qi, J., Chehbouni, A., Huete, A.R., Keer, Y.H., & Sorooshian, S. (1994). A modified soil vegetation adjusted index. *Remote Sensing of Environment*, *48*, 119–126.

Rabaglia, R.J., Dole, S.A., & Cognato, A.I. (2006). Review of American Xyleborina (Coleoptera: Curculionidae: Scolytinae) occurring north of Mexico, with an illustrated key. *Annals of the Entomological Society of America*, *99*, 1034–1056.

Raikes, C., & Burpee, L.L. (1998). Use of multispectral radiometry for assessment of rhizoctonia blight in creeping bentgrass. *Phytopathology*, *88*, 446–449.

Ray, S.S., Jain, N., Miglani, A., Singh, J.P., Singh, A.K., Panigrahy, S., & Parihar, J.S. (2010). Defining optimum spectral narrow bands and bandwidths for agricultural applications. *Current Science*, *98*, 1365–1369.

Rogan, J., Franklin, J., Stow, D., Miller, J., Woodcock, C., & Roberts, D. (2008). Mapping land-cover modifications over large areas: A comparison of machine learning algorithms. *Remote Sensing of Environment*, *112*, 2272–2283. http://dx.doi.org/10.1016/j.rse.2007.10.004.

Rondeaux, G., Steven, M., & Baret, F. (1996). Optimization of soil-adjusted vegetation indices. *Remote Sensing of Environment*, *55*, 95–107.

Rougean, J.L., & Breon, F.M. (1995). Estimating PAR absorbed by vegetation from bidirectional reflectance measurements. *Remote Sensing of Environment*, *51*, 375–384.

Rouse, J.W., Haas, R.H., Schell, J.A., & Deering, D.W. (1973). Monitoring vegetation systems in the Great Plains with ERTS. *Proceedings of the Earth Resources Technology Satellite Symposium NASA SP-351, Washington, DC, USA. Vol. 1*. (pp. 309–317).

Rzempoluck, E.J. (1997). *Neural network data analysis using Simulnet*. Burnaby. B.C. Canada: Simon Fraser University0-387-98255-8, 1–3 (13–75).

Sankaran, S., Ehsani, R., Inch, S.A., & Ploetz, R.C. (2012). Evaluation of visible-near infrared reflectance spectra of avocado leaves as a non-destructive sensing tool for detection of laurel wilt. *Plant Disease*, *96*, 1683–1689.

Sankaran, S., Khot, L.R., Maja, J.M., & Ehsani, R. (2013). Comparison of two multiband cameras for use on small UAVs in agriculture. *5th IEEE Workshop on Hyperspectral Image and Signal Processing: Evolution in Remote Sensing (WHISPERS), 25–28 June, Gainesville, FL*.

Sankaran, S., Mishra, A., Ehsani, R., & Davis, C. (2010). A review of advanced techniques for detecting plant diseases. *Computers and Electronics in Agriculture*, *72*, 1–13.

Smith, A.M.S., Drake, N.A., Wooster, M.J., Hudak, A.T., Holden, Z.A., & Gibbsons, C.J. (2007). Production of Landsat ETM+ reference imagery of burned areas within Southern African savannahs: Comparison of methods and application to MODIS. *International Journal of Remote Sensing*, *28*, 2753–2775.

Smith, G.M., & Milton, E.J. (1999). The use of the empirical line method to calibrate remotely sensed data to reflectance. *International Journal of Remote Sensing*, *20*, 2653–2662.

SPSS v.22 (2014). *IBM SPSS Statistics 22 documentation*. Microsoft Corp.: Redmond, WA Reference book.

Suárez, L., Zarco-Tejada, P.J., González-Dugo, V., Berni, J.A.J., Sagardoy, R., Morales, F., & Fereres, E. (2010). Detecting water stress effects on fruit quality in orchards with time-series PRI airborne imagery. *Remote Sensing of Environment*, *114*, 286–298.

Thenkabail, P.S., Lyion, J.G., & Huete, A. (2012). In CRC Press (Ed.), *Hyperspectral remote sensing of vegetation*. Boca Raton, FL: Taylor and Francis Group (Chapter 14).

Torres-Sánchez, J., López-Granados, F., De Castro, A.I., & Peña-Barragán, J.M. (2013). Configuration and specifications of an unmanned aerial vehicle (UAV) for early site specific weed management. *PLoS ONE*, *8*, e58210.

USDA (2009, April). Census of agriculture, Florida: State and county data. *Graphic area series, Part 9*, *Vol. 1*, Washington, D.C.: United States Department of Agriculture, National Agricultural Statistics Service (http://www.agcensus.usda.gov/Publications/2007/Full_Report/Volume_1,_Chapter_1_State_Level/Florida/flv1.pdf. Accessed 22 May 2015).

USDA (2013). *Noncitrus fruits and nuts: 2013 Summary, 1948–2698. July 2014.* Washington, D.C.: National Agricultural Statistic Service, United States Department of Agriculture (http://usda.mannlib.cornell.edu/usda/current/NoncFruiNu/NoncFruiNu-07-17-2014_revision.pdf. Accessed 8 March 2015).

USDA. Forest Service (2014). Forest Health Protection. *Laurel Wilt Information* (http://www.fs.fed.us/r8/foresthealth/laurelwilt/dist_map.shtml. Accessed 9 January 2015).

Usha, K., & Singh, B. (2013). Potential applications of remote sensing in horticulture — A review. *Scientia Horticulturae*, *153*, 71–83.

Wu, N., Liu, J., Zhou, G., Yan, R., & Zhang, L. (2012). Prediction of chlorophyll content of leaves of oil camelliae after being infected with anthracnose based on Vis/NIR spectroscopy. *Spectroscopy and Spectral Analysis*, *32*, 1221–1224.

Zhang, M., Qin, Z., & Liu, X. (2005). Remote sensed spectral imagery to detect late blight in field tomatoes. *Precision Agriculture*, *6*, 489–508.